macromol

MDPI

Article

Anti-Inflammatory Activities of *Zophobas morio* Larvae Lipids on Lipopolysaccharide-Induced Activated Macrophages: Reprogramming Macrophage Polarization and Attenuating Oxidative Stress

Ju-Hwi Park [1,†], Ha-Seong Cho [1,†], Ju-Ock Nam [1,2,3,*] and Won-Young Lee [1,2,3,*]

[1] School of Food Science and Biotechnology, Kyungpook National University, Daegu 41566, Republic of Korea; qkrwn9809@gmail.com (J.-H.P.); hasung31694@knu.ac.kr (H.-S.C.)
[2] Research Institute of Tailored Food Technology, Kyungpook National University, Daegu 41566, Republic of Korea
[3] Department of Biomedical Technology, School of Convergence, Kyungpook National University, Daegu 41566, Republic of Korea
* Correspondence: namjo@knu.ac.kr (J.-O.N.); wonyoung@knu.ac.kr (W.-Y.L.); Tel.: +82-53-950-7760 (J.-O.N.); +82-53-950-7761 (W.-Y.L.)
† These authors contributed equally to this work.

Abstract

This study investigated the structural and anti-inflammatory properties of *Zophobas morio* lipids (ZMLs). The fatty acid (FAs) composition showed a higher proportion of unsaturated FAs, mainly consisting of oleic (30.30%) and linoleic acids (20.05%), than saturated FAs, including palmitic (24.80%) and stearic acids (12.96%). In addition, FT-IR and ^{1}H-NMR analyses confirmed that ZML possessed a typical triglyceride structure, with long-chain alkyl groups. Thermogravimetric analysis (TGA) indicated that ZML exhibited high thermal stability, with a degradation peak at 369 °C. Differential scanning calorimetry (DSC) displayed a thermal transition at −8 °C, corresponding to the crystallization of unsaturated FAs in ZML. ZML significantly inhibits lipopolysaccharide (LPS)-induced pro-inflammatory M1 macrophage polarization by suppressing nuclear factor κB (NF-κB) and mitogen-activated protein kinase (MAPK) signaling pathways, thereby attenuating the expression of inflammatory mediators. Additionally, ZML alleviated inflammatory oxidative stress by activating the nuclear factor erythroid 2-related factor 2 (Nrf2)-mediated antioxidant pathway. Notably, ZML not only induced M2 macrophage polarization in quiescent macrophages but also reprogrammed M1 macrophages toward the anti-inflammatory M2 phenotype. These findings suggest that ZML is a natural nutritional lipid source and a potential therapeutic agent for modulating inflammatory response.

Keywords: anti-inflammatory; anti-oxidant; fatty acids; macrophage; polarization; *Zophobas morio* lipid

Check for updates

Academic Editors: Ana María Díez-Pascual and Eleonora Marsich

Received: 26 February 2026
Revised: 16 March 2026
Accepted: 3 April 2026
Published: 6 April 2026

Copyright: © 2026 by the authors. Licensee MDPI, Basel, Switzerland. This article is an open access article distributed under the terms and conditions of the Creative Commons Attribution (CC BY) license.

1. Introduction

Macrophages are representative innate immune cells distributed throughout the body and are involved in nearly all facets of immunological responses [1,2]. Under normal conditions, macrophages exist in a quiescent state, but upon exposure to foreign stimuli, they become activated and express various immunological modulators (e.g., nitric oxide, prostaglandin E2, and pro-inflammatory cytokines), which play pivotal roles in

host immunity [1,3]. Nitric oxide, produced by inducible nitric oxide synthase (*iNOS*), regulates hypertension, blood flow regulation, and antimicrobial properties [4]. In addition, PGE2, generated by cyclooxygenase-2 (*COX-2*), promotes local migration and activation of various immune cells [5]. Tumor necrosis factor alpha (TNF-α) and interleukin-6 (IL-6) are the representative pro-inflammatory cytokines that trigger immune responses, promote other immune cell differentiation, and reinforce macrophage phagocytosis activity [6]. The adequate and controlled expression of immunological mediators is essential; however, their overexpression can lead to inflammatory diseases and tissue damage, thereby acting as inflammatory mediators [7]. Therefore, numerous studies have suggested that agents that ameliorate the overexpression of inflammatory mediators could function as anti-inflammatory therapies [8].

Over the past few decades, interest in edible insects as an alternative food resource has grown substantially, driven by their numerous advantages, including high nutritional value and low environmental burden [9,10]. Edible insects offer several advantages over conventional animal-derived protein sources, including lower energy expenditure and water requirements, smaller land area required for cultivation, and lower greenhouse gas emissions [11]. Among edible insects, *Zophobas morio*, commonly known as the super mealworm, has garnered widespread attention for its high protein content [12,13]. Accordingly, previous studies have focused on using *Z. morio* protein to investigate its techno-functional properties (e.g., emulsion properties and protein digestibility) and its biological properties, including antioxidant and immunological activities [12–15]. Although proteins from *Z. morio* are primarily highlighted, the disposal of lipids as by-products after the defatting process also has noticeable nutritional value [16].

Crucially, the presence of key macronutrient components, including essential amino acids, unsaturated fatty acids, and minerals, confers various biological properties, such as antioxidant, immunomodulatory, and antidiabetic effects [10,17]. Among these components, lipids are particularly noteworthy; they constitute the second-largest proportion of *Z. morio* after proteins and are rich in polyunsaturated fatty acids, such as omega-3 and omega-6 fatty acids [18,19]. The high content of these fatty acids is comparable to that of fish, thereby positioning insect lipids as an alternative source of essential fatty acids [20,21]. Despite the well-known anti-inflammatory properties of lipids from various natural sources, studies investigating lipids from *Z. morio* remain insufficient [22–25]. Therefore, this study aimed to characterize the structural properties of *Z. morio* lipid (ZML) and elucidate its anti-inflammatory properties and underlying mechanisms.

2. Materials and Methods

2.1. Zophobas morio Lipid (ZML) Extraction

Zophobas morio used in this study was obtained from a cricket farm (Suwon, Republic of Korea). The material was dried and ground using a grinder (RT-04, Mill powder, Tainan, Taiwan) for 30 s. The ZML was extracted from the sample according to the method outlined in the previous study of [26] with slight modifications. Briefly, 1.2 g of ZM powder was mixed with a solution containing chloroform (Duksan Chemicals, Ansan, Republic of Korea) and methanol (Duksan Chemicals) at a ratio of 2:1 (v/v), followed by the addition of 10 mL of distilled water. The mixture was thoroughly vortexed and kept at 25 °C for 20 min. Subsequently, the lower phase (chloroform) was separated from the mixture using a funnel and vacuum-filtered. The ZML was obtained by concentrating the collected phase using nitrogen blowing and kept in a sealed vial at −80 °C until use. The extraction yield and density of ZML were 24.4 ± 2.6% and 0.928 ± 0.011 g/mL, respectively (based on wet/dry at 25 °C). For the in vitro anti-inflammatory assays, ZML was dissolved in dimethyl sulfoxide (DMSO) to a stock concentration of 200 mg/mL.

2.2. Fatty Acid Profile

The fatty acids (FAs) composition of ZML was determined after a methyl-ester derivation process. The transesterification was carried out following the method described by Stark et al. [27] with modifications. The ZML (200 µL) was dissolved with 6% sulfuric acid in methanol and placed in a water bath (Daihan Scientific Co., Ltd., Wonju, Republic of Korea) at 90 °C for 90 min. After heating, 2 mL of petroleum ether was added, and the mixture was centrifuged at 2000 rpm for 10 min to extract fatty acid methyl esters (FAMEs). The upper phase was recovered from the mixture and dried under a nitrogen atmosphere. Subsequently, 800 µL of n-hexane was added to the dried FAME mixture, which was then injected into a gas chromatography–mass spectrometry system (GC-MS QP2010 Plus, Shimadzu Corp., Kyoto, Japan). In this case, the GC oven was equipped with an HP-INNOWAX capillary column 30 m × 0.25 mm i.d., 0.25 µm (Agilent Technologies, Palo Alto, CA, USA). The GC conditions were: an injection temperature of 260 °C; an injection volume of 2 µL with a split ratio of 1:10; a helium flow rate of 1 mL/min; and a temperature program comprising an initial oven temperature of 170 °C, increased to 260 °C at a rate of 5 °C/min, and held for 10 min [28]. Mass acquisitions were performed at 70 eV (EI), scanning the range 40–500 m/z at 220 °C.

The FAME standard mixture (Sigma-Aldrich Co., St. Louis, MO, USA) was used to identify the detected peaks, and the linear retention index (LRI) was calculated using alkane standards (Sigma-Aldrich) under the same conditions. The relative FA composition was expressed as a percentage of the signal peak areas [19].

2.3. Structural Analyses of ZML

2.3.1. Fourier Transform Infrared Spectroscopy (FT-IR)

FT-IR analysis was conducted using an FT-IR spectrophotometer (Frontier, PerkinElmer, Waltham, MA, USA). The spectrum of ZML was scanned in the 400–4000 cm^{-1} range with 16 scans at a resolution of 4 cm^{-1}.

2.3.2. ^{1}H-NMR Analysis

The nuclear magnetic resonance (NMR) experiment was conducted using a Bruker spectrometer (Billerica, MA, USA) equipped with a 5 mm probe at 298 K. For ^{1}H-NMR analysis, 50 µL of ZML was dissolved in 500 µL of chloroform-d ($CDCl_3$) and transferred to a 5 mm NMR tube without filtration [29]. ^{1}H-NMR spectra of ZMP were recorded at 500 MHz for 64 scans. The acquired spectra were processed and analyzed using TOPSPIN software, version 4.1 (Bruker, Rheinstetten, Germany).

2.4. Thermal Properties Analysis

2.4.1. Thermogravimetric Analysis (TGA) and Derivative Thermogravimetric (DTG) Analysis

A thermogravimetric analyzer (Discovery SDT 650, TA Instruments, New Castle, DE, USA) was used to investigate the mass loss of ZML during thermal treatment. Approximately, 20 mg of ZML was loaded on the stainless-steel pan and hermetically sealed. Then, the sample was heated from 25 to 600 °C at a rate of 10 °C/min [30]. The run was conducted under nitrogen flushing at 20 mL/min^{-1}.

2.4.2. Differential Scanning Calorimetry (DSC)

The crystallization and melting point of ZML were analyzed using a thermal analysis system (Q2000; TA Instruments, New Castle, DE, USA) following the method described by Cha et al. [31]. The ZML (10 mg) was sealed in an aluminum pan and placed under a nitrogen atmosphere at a flow rate of 20 mL min^{-1}. The temperature was programmed to increase from −60 °C to 60 °C at a rate of 10 °C/min^{-1}. The temperature was held

isothermally at 60 °C for 1 min. Subsequently, a quick cooling program was performed to equilibrate the temperature at −60 °C. Thermogram parameters, including onset temperature (T_o), denaturation temperature (T_d), and enthalpy (ΔH), were determined using TA Universal analysis 2000 software [32].

2.5. Cell Culture and Cell Viability Analysis

The murine origin macrophage cell line RAW264.7 was obtained from the Korean Cell Line Bank (Seoul, Republic of Korea). Cells were maintained in Dulbecco's Modified Eagle Medium (Gibco, Grand Island, NY, USA) supplemented with 10% fetal bovine serum with 1% penicillin/streptomycin. The cells were maintained in a humidified atmosphere at 37 °C with 5% CO_2. The same medium conditions were consistently applied for all subsequent in vitro experiments to ensure stable cellular metabolism and physiological responses.

The Cell Counting Kit-8 (CCK-8; Dojindo, Kumamoto, Japan) assay was performed to assess cell viability. RAW264.7 cells were seeded and treated with 200–800 μg/mL of ZML for 24 h, with the final DMSO concentration maintained at 0.4% (*v*/*v*) in all treatment groups. Subsequently, 10 μL of CCK-8 solution was incubated for 2 h, and the absorbance was measured at 450 nm using a SPECTROstar Nano microplate reader (BMG Labtech, Ortenberg, Germany). The cell viability was normalized using the following Equation (1):

$$\text{Cell viability } (\%) = \frac{\textit{Absorbance in Experimental group}}{\textit{Absorbance in Non–treatment group}} \times 100 \quad (1)$$

2.6. Nitric Oxide Synthesis Assay

The Griess reagent assay (Promega, Madison, WI, USA) was performed to analyze nitric oxide synthesis. RAW264.7 cells were pretreated with 200–800 μg/mL of ZML for 1 h, and then co-treated with lipopolysaccharide (LPS) for 24 h. Subsequently, the supernatants were collected after sequential treatment with the sulfanilamide solution and the N-(1-naphthyl) ethylenediamine solution, with a 10 min interval between treatments. Absorbance was measured at 570 nm using a SPECTROstar Nanomicroplate reader. The nitric oxide concentration was quantified using a standard curve established with sodium nitrite ($NaNO_2$) dissolved in the same culture medium (Figure S1).

2.7. Western Blot Assay

The cell lysates were prepared using Radioimmunoprecipitation assay buffer supplemented with 1% protease inhibitor and phosphatase inhibitor. The lysates were separated using a sodium dodecyl sulfate–polyacrylamide gel electrophoresis and transferred to the membrane. The membrane was blocked with 5% skim milk dissolved in Tris-buffered saline containing 0.1% Tween 20 (TBST), and then incubated overnight with primary antibodies (Table S1). Subsequently, the membranes were washed with TBST and incubated with secondary antibodies for 1 h. After washing under identical conditions, the enhanced chemiluminescence detection kit (Cytiva, Marlborough, MA, USA) was used to quantify protein expression. Finally, protein expression was normalized using ImageJ (version 1.54p, NIH, USA).

2.8. Real-Time Quantitative Polymerase Chain Reaction (RT-qPCR)

Total RNA was isolated using the RNAiso Plus Reagent (TaKaRa Bio, Kusatsu, Japan), and complementary DNA (cDNA) was synthesized using ReverTraAce^{TM} qPCR Master Mix (TOYOBO, Osaka, Japan). RT-qPCR was performed with the Cycler iQ^{TM} Real-Time PCR Detection System (Bio-Rad Laboratories, Hercules, CA, USA) using SYBR Green (TOYOBO) and specific primers (Table S2). The relative mRNA expression of *tnfα*, *il6*, *il10*, and *Arg1* was normalized to that of *bactin* and calculated using the $2^{-\Delta\Delta Ct}$ method.

2.9. Enzyme-Linked Immunosorbent Assay (ELISA)

The supernatants from the samples were collected and then centrifuged. Then, the secretion of TNF-α, IL-6, and prostaglandin E2 was measured using ELISA KITS (R&D Systems, Minneapolis, MN, USA) according to the manufacturer's instructions.

2.10. Flow Cytometry Assay

All flow cytometry analysis was performed using an Attune Acoustic Focusing Cytometer (Thermo Fisher Scientific, Waltham, MA, USA).

2.10.1. Cell Surface Marker Analysis

Analysis of cell surface marker (CD80 and CD206) expression was performed following the study by Park et al. [33] with some modifications. The cells were collected and incubated with anti-cluster of differentiation (CD) 16/32 antibody (eBioscience, San Diego, CA, USA) for 20 min to block nonspecific antibody binding. Then, cells were stained with anti-CD80-PE (eBioscience) or anti-CD206-FITC (eBioscience) for 40 min. Subsequently, the cells were recovered, and flow cytometry was performed. The $CD80^+$ area or $CD206^+$ area was quantified under excitation/emission (Ex/Em) = 488/574 nm and Ex/Em = 488/530 nm conditions.

2.10.2. Intracellular Reactive Oxygen Species Production Analysis

Reactive oxygen species (ROS) analysis was performed using 2′, 7′-dichlorofluorescein diacetate (DCF-DA) analysis based on the previous study conducted by Aliya et al. The cells were exposed to a 20 μM DCF-DA solution and incubated for 30 min. Subsequently, the cells were recovered, and flow cytometry was performed. The $DCF\text{-}DA^+$ area was quantified under Ex/Em = 488/530 nm conditions.

2.11. Statistical Analysis

All experiments were performed in at least three independent biological replicates (n = 3), and each sample was analyzed in technical triplicate. The data were presented as mean ± standard deviation. Statistical significance was analyzed using one-way analysis of variance (ANOVA), followed by Dunnett's post hoc test for multiple comparisons between groups, using SPSS software (version 20.0; IBM Corp., Chicago, IL, USA). $p < 0.05$ was considered statistically significant.

3. Results

3.1. Fatty Acids Profile of ZML

The identified and relative composition ratios of fatty acids (FAs) of ZML are presented in Table 1. The result presents a higher proportion of unsaturated fatty acids (UFAs) (56.53%) than saturated fatty acids (SFAs) (43.46%) in ZML. Specifically, the UFAs of ZML consist mainly of monounsaturated FAs, such as oleic acid (30.30%), and polyunsaturated FAs, including linoleic acid (20.05%). Among SFAs, palmitic (24.80%) and stearic acid (12.96%) were the most abundant.

The FA profile of ZML is similar to that reported by Rafael et al. [19], who observed a higher content of UFAs (54.46%) than of SFAs (45.54%) in oil extracted from *Zophobas morio* using the Soxhlet method. In addition, the representative FAs' composition (oleic, linoleic, palmitic, and stearic acid) determined in ZML is also detected as a major compound of lipids extracted from *Tenebrio molitor*, *Acheta domesticus*, and *Locusta migratoria* [34]. However, variations in the relative proportions of UFAs and SFAs have been reported across different studies, which may be attributed to differences in insect species or processing methods [19,35].

Notably, ZML contains linoleic acid (*n*-6) and α-linolenic acid (*n*-3), which are known for their nutritional importance in the diet. Since the human body does not synthesize them, they can be obtained through consumption [36]. In addition, these FAs have been reported for their significant anti-inflammatory effects [37]. In summary, the largely discarded ZML as a by-product has a potential functional source in the food fortification and pharmaceutical fields.

Table 1. Fatty acid profile of *Zophobas morio* lipid.

No.	Fatty Acid		%	LRI[1]	LRI[2]
1	Caprylic acid	C8:0	2.70 ± 0.48	1311.96	1306.22
2	Myristic acid	C14:0	1.99 ± 0.35	1922.80	1920.81
3	Palmitic acid	C16:0	24.80 ± 1.71	2129.13	2120.56
4	Palmitoleic acid	C16:1	3.37 ± 0.42	2150.87	2155.15
5	7,10-hexadecadienoic acid	C16:2	1.30 ± 0.25	2199.55	-
6	Margaric acid	C17:0	1.03 ± 0.20	2230.15	2227.76
7	Stearic acid	C18:0	12.96 ± 1.19	2333.51	2330.62
8	Oleic acid	C18:1	30.30 ± 1.09	2357.47	2353.59
9	Linoleic acid	C18:2	20.05 ± 0.38	2406.65	2403.33
10	α-Linolenic acid	C18:3	1.51 ± 0.30	2473.80	2478.92
	Σ Saturated fatty acids		43.48 ± 0.50		
	Σ Unsaturated fatty acids		56.53 ± 0.50		
	Σ Monounsaturated fatty acids		33.67 ± 0.67		
	Σ Polyunsaturated fatty acids		22.86 ± 0.17		
	Total		100.00		

Note: LRI[1] and LRI[2] denote the linear retention indices of ZML and the standard, respectively.

3.2. Structural Analysis of ZML

3.2.1. FT-IR Analysis

FT-IR analysis was conducted to investigate the primary structure of ZML. The FT-IR spectra of ZML within the range from 400 to 4000 cm^{-1} are shown in Figure 1a and Table S3. The observed peak at 3006 cm^{-1} was attributed to a carbon double bond (C=C), which indicated the presence of unsaturated FAs in ZML [38]. The characteristic absorption peaks at 2854 and 2924 cm^{-1} were associated with the stretching bands of CH_2 and CH_3, suggesting the presence of long-chain alkyl groups in ZML, while the prominent peak at 1744 cm^{-1} indicated the stretching vibration of -C-O groups in triglycerides [39]. The "fingerprint" region, ranging from 700 to 1500 cm^{-1}, was characterized according to the relative proportion of SFA and UFA acyl groups, reflecting structural variances and differences in FA compositions among different lipids [30,40]. The peaks at 1378 and 1463 cm^{-1} might be assigned to scissoring and symmetric bending vibrations of aliphatic CH_2 and CH_3 groups, respectively [30]. The band observed at 722 cm^{-1} corresponded to a weak rocking vibration, which was caused by -$(CH_2)_n$-(CH_3) groups [41]. These results are further supported by the results of GC-MS, where the various compositions of SFA and UFA were identified in the ZML. In addition, several FT-IR analyses on the lipid obtained from edible insects, such as *Bombys mori* and *Speciomerus ruficornis*, also displayed similar patterns of bands and assignments to ZML in this study [30,38].

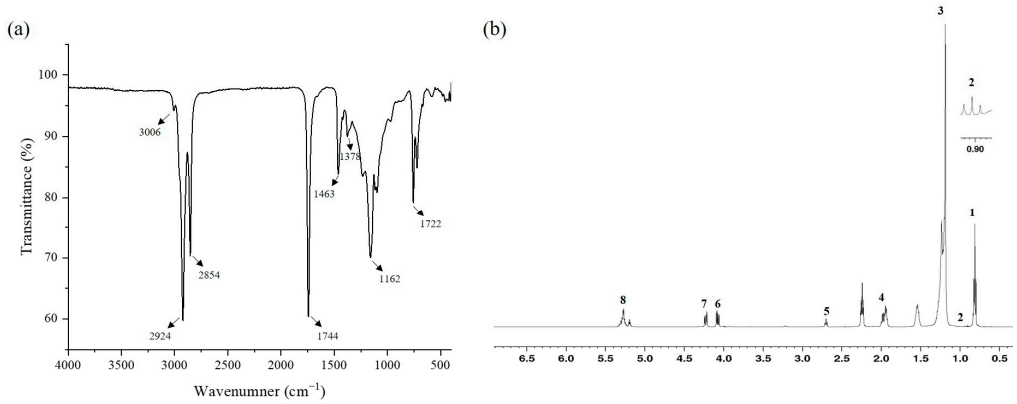


Figure 1. Structural characterization of *Zophobas morio* lipid: (**a**) FT-IR and (**b**) ^{1}H-NMR. The peak assignments for FT-IR and ^{1}H-NMR are detailed in Table S3 and Table S4, respectively.

3.2.2. ^{1}H-NMR Profile

^{1}H-NMR spectra and the assignments of the distinct proton signals of ZML are presented in Figure 1b and Table S4, respectively. The ^{1}H-NMR spectrum of the ZML displayed a broad resonance signal in the range of 0.78–0.83 ppm, indicating the terminal methyl proton (-CH_3), whereas a relatively weak signal at approximately 0.90 ppm was attributed to the *n*-3 fatty acids, such as α-linolenic acid [29]. The characteristic signal around 1.2 ppm was assigned to the long aliphatic chains, -$(CH_2)_n$-, present in all FAs [42]. Signals observed at 1.92–2.00 and 2.69–2.71 ppm indicated the presence of oleic and linoleic acid, respectively [43]. The observed doublet signals between 4.06 and 4.24 ppm demonstrated the triglyceride structure of ZML. In addition, proton signals corresponding to olefinic (CH=CH) groups of unsaturated fatty acids were observed in the range of 5.23–5.32 ppm [29]. Overall, the ^{1}H-NMR profile was consistent with the obtained results of GC-MS and FT-IR, confirming the structural characteristics of ZML.

3.3. Thermal Properties of ZML

Investigating the thermal behavior of lipids is essential for their effective industrial application. The TGA and DTG curves of ZML were analyzed to investigate the effects of increasing temperature in the range of 20–600 °C (Figure 2a). The TGA and DTG curves describe the thermal weight loss in a single degradation phase at temperatures between 150 and 450 °C. Notably, the initial decomposition temperature (T_{onset}) and peak temperature (T_{peak}) were observed at 369 °C and 411 °C, respectively. These results could be attributed to the typical degradation temperature of triglycerides (380–480 °C) [44]. Additionally, the total mass of ZML (95.70%) was lost at 600 °C. Moreover, the FA profile properties, such as the proportion of SFA to UFA and the length of the FA chain, could also contribute to the thermal stability of ZML [30].

The melting and crystallization behaviors of ZML are presented in Figure 2b. During heating, two endothermic peaks were observed for ZML at −7.38 °C and 5.00 °C, respectively. In contrast, for cooling, only one exothermic peak was identified at −8.03 °C. These thermal transitions at low temperatures could be due to its higher UFA content compared to SFA. Less ordered crystalline structures and weaker intermolecular interactions of UFA than SFA could contribute to lower crystallization temperatures [45].

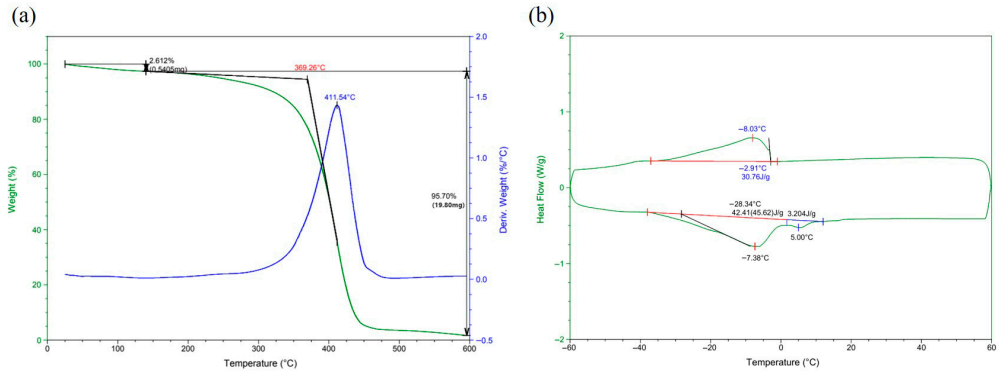


Figure 2. Thermal properties of *Zophobas morio* lipid: (**a**) thermogravimetric curve (Green), derivative thermogravimetry curve (Blue), and measurement line (Black); (**b**) differential scanning calorimetry analyses.

3.4. ZML Alleviated Inflammatory Mediator Expressions in LPS-Induced M1 Polarization in Macrophages

Prior to confirming the anti-inflammatory properties, a cell viability assay was performed to assess cytotoxicity at test concentrations (200–800 μg/mL) of ZML (Figure S2). Compared to the control group (100 ± 5.69%), ZML treatment significantly increased the cell viability of RAW264.7 cells (126.26–132.97%). The result indicated that under test concentrations, ZML exhibited no cytotoxicity but also induced macrophage proliferation. For the subsequent experiments, concentrations ranging from 200 to 800 μg/mL were utilized.

LPS, a component of the Gram-negative bacterial outer membrane, is widely recognized as a stimulus for macrophage activation, thereby triggering inflammatory responses [46]. Based on the previous finding, the LPS-induced activated macrophage model was utilized to mimic the inflammatory status of macrophages and confirm whether ZML could alleviate it. Figure 3 denotes the effect of ZML on the expression of LPS-induced macrophage-derived inflammatory mediators. Notably, LPS exposure significantly upregulated the secretion of nitric oxide and PGE2 (24.71 ± 0.98 μM and 29.97 ng/mL), which was mitigated by ZML treatment in a dose-dependent manner (19.67–2.26 μM and 26.06–14.94 ng/mL) (Figure 3a,b). The corresponding results for iNOS and COX-2 were also confirmed: ZML treatment significantly mitigated LPS-induced upregulation of iNOS and COX-2 expression (0.52–0.00-fold and 0.76–0.08-fold) compared to the LPS-only treatment group (1.00 ± 0.07-fold and 1.00 ± 0.09-fold) (Figure 3c). The result suggests that ZML treatment mitigated the increased secretion of nitric oxide and PGE2 by decreasing the expression of iNOS and COX-2. Also, as shown in Figures 3d and S3, a similar trend was observed in pro-inflammatory cytokine expression: LPS treatment significantly upregulated *tnfα* and *il6* mRNA expression (1.00 ± 0.07-fold and 1.00 ± 0.09-fold), which was mitigated by ZML treatment (0.87–0.65-fold and 0.30–0.00-fold). The concurrent results of proinflammatory cytokine secretion showed that LPS treatment significantly upregulated TNF-α and IL-6 secretion (16.08 ± 1.19 ng/mL and 6.16 ± 0.17 ng/mL), which was mitigated by ZML treatment (14.95–10.98 ng/mL and 5.89–1.78 ng/mL). The results suggest that ZML treatment ameliorates LPS-induced upregulation of pro-inflammatory cytokines. This aligns with the previous studies conducted by Huang et al. [47], who confirmed the anti-inflammatory properties of *Perilla frutescens* leaf extract by alleviating LPS-induced upregulation of inflammatory mediators.

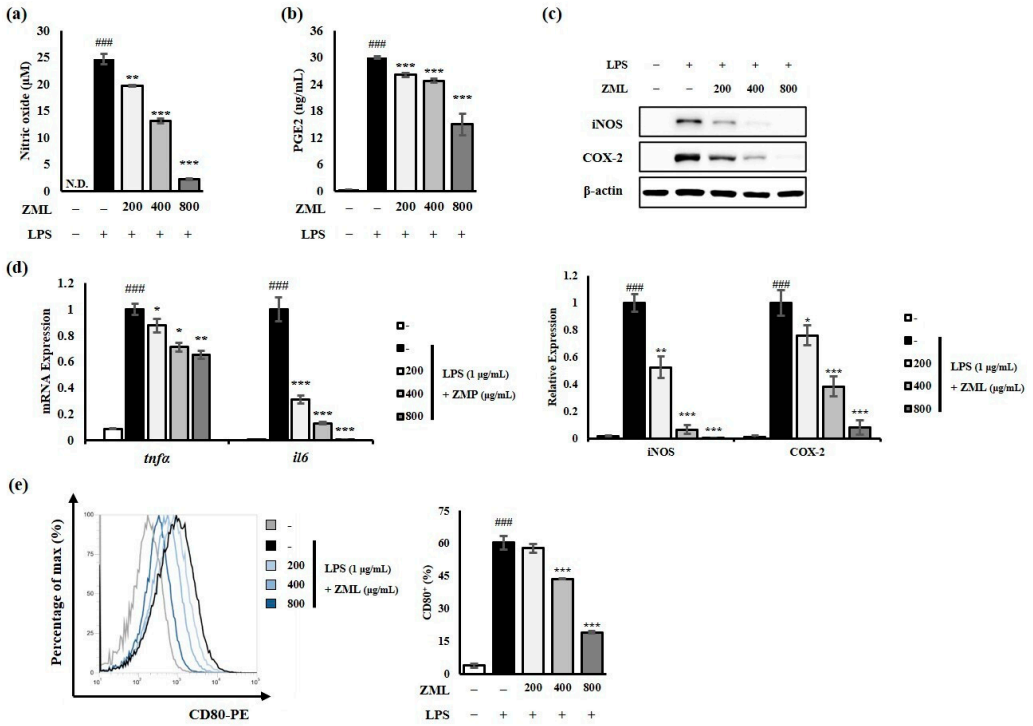


Figure 3. *Zophobas morio* lipid (ZML) alleviated LPS-induced inflammatory responses in macrophages. RAW264.7 cells were pretreated with ZML for 1 h, followed by co-treatment with LPS (1 μg/mL) for 24 h, and then nitric oxide synthesis (**a**), prostaglandin E2 (PGE2) secretion (**b**), expression of inducible nitric oxide synthase (iNOS) and cyclooxygenase-2 (COX-2) (**c**), mRNA expression of pro-inflammatory cytokines (**d**), and CD80 expression (**e**) were analyzed using Griess reagent assay, ELISA, Western blot, RT-qPCR, and flow cytometry analysis. ### $p < 0.001$ compared with the non-treatment group and the LPS-only treatment group. * $p < 0.05$, ** $p < 0.01$, and *** $p < 0.001$ compared with the LPS + ZML co-treatment group and the LPS-only treatment group.

During an inflammatory state, macrophages highly express the cell surface molecule CD80 [13]. This acts as a co-stimulatory factor by binding to CD28 on T cells, thereby facilitating antigen presentation and further inducing the inflammatory response [48]. Therefore, CD80 is widely recognized as a biomarker of M1 macrophage polarization, the pro-inflammatory phenotypic macrophage [49]. Accordingly, numerous studies have reported that decreased CD80 expression on activated macrophages indicates the alleviation of M1 macrophage polarization, thereby suggesting a reduction in the inflammatory response [48,50]. Figure 3e denotes the effects of ZML on LPS-induced M1 macrophage polarization. LPS exposure significantly increased CD80 expression on the surface of RAW264.7 cells (60.35 ± 3.18%) compared to the non-treatment group (3.89 ± 0.95%), suggesting successful M1 polarization conducted by LPS treatment. Likewise, ZML treatment significantly reduced LPS-induced CD80 upregulation (57.88–19.19%), suggesting that ZML treatment ameliorated M1 macrophage polarization. This result aligns with the previous study by Shiratori et al. [51], which suggested that decreased CD80 expression was associated with ameliorating M1 macrophage polarization. Taken together, the results demonstrate that ZML treatment dramatically reduces the expression of LPS-induced inflammatory mediators and ameliorates M1 macrophage polarization, highlighting the anti-inflammatory properties of ZML.

3.5. ZML Downregulated NFκB/MAPK Signaling in LPS-Induced Activated Macrophages

Upon LPS exposure, macrophages are activated via intracellular signaling pathways, most notably the nuclear factor-kappa B (NFκB) and mitogen-activated protein kinase (MAPK) pathways [46]. NFκB signaling is mediated by inhibitory kappa B and NFκB. In

the basal state, NFκB is sequestered in the cytoplasm by inhibitory kappa B (IκB), which interferes with its translocation into the nucleus [52]. However, upon activation, IκB is phosphorylated and undergoes a conformational change, leading to its dissociation from NFκB. This allows NFκB to translocate into the nucleus and function as a transcriptional factor, leading to the expression of inflammatory mediators, including iNOS, COX-2, and pro-inflammatory cytokines [3]. Concurrently, MAPK signaling, comprising p38, extracellular signal-regulated kinase (ERK), and c-Jun N-terminal kinase (JNK), is activated through phosphorylation upon LPS stimulation [53]. This signaling cascade triggers the nuclear translocation of activator protein-1, which promotes the expression of aforementioned inflammatory mediators [53,54]. Therefore, attenuation of the LPS-induced NFκB and MAPK signaling pathways is expected to alleviate macrophage activation, thereby exerting anti-inflammatory properties [55].

Figures 4a,b and S4a showed the effects of ZML on the LPS-induced upregulated NFκB signaling pathway. LPS treatment induced the phosphorylation of IκB and NFκB (1.00 ± 0.03-fold and 1.00 ± 0.10-fold), accompanied by a decrease in cytosolic NFκB levels and a concomitant increase in nuclear NFκB expression (1.00 ± 0.10-fold and 1.00 ± 0.29-fold), normalized to the non-treatment group (0.02 ± 0.02-fold, 0.11 ± 0.10-fold, 0.23 ± 0.10-fold, and 6.15 ± 0.86-fold, respectively). These results indicate the activation of the NFκB signaling pathway, which was attenuated by ZML treatment. ZML downregulated the phosphorylation of IκB (0.79–0.45-fold) and NFκB (0.71–0.41-fold) compared to the LPS-only treatment group. Furthermore, ZML reversed the LPS-induced nuclear translocation of NFκB by restoring its cytosolic levels (1.60–2.42-fold) and reducing its nuclear levels (0.89–0.51-fold) compared to the LPS-only treatment group. These results confirm that ZML inhibits the LPS-induced NFκB signaling pathway. A similar result was observed in the MAPK signaling pathway. LPS treatment significantly increased the phosphorylation of p38, ERK, and JNK, which was dramatically attenuated by ZML treatment (Figure 4c). Notably, ZML treatment downregulated the phosphorylation levels of p38 to 0.82–0.44-fold, ERK to 0.81–0.45-fold, and JNK to 0.86–0.25-fold, respectively. These results align with those of the study by Rod-In et al. [22], which demonstrated the anti-inflammatory properties of *Arctoscopus japonicas* egg-derived lipids.

3.6. ZML Upregulated MAPK-Nrf2/HO-1 Signaling in Macrophage

Reactive oxygen species (ROS) produced in macrophages play crucial roles in the immune system, including pathogen eradication and regulation of the macrophage activation signaling pathway [56]. However, during inflammation, intracellular ROS are excessively produced, and accumulated ROS lead to oxidative stress, resulting in cytotoxicity and inflammatory disorders [57]. Therefore, confirming alleviation of oxidative stress during inflammation further validates the agent's anti-inflammatory activity. Figure 5a denotes the effects of ZML on the mitigation of LPS-induced oxidative stress in macrophages. Notably, LPS exposure significantly increased DCF-DA^{+} area (34.34 ± 2.79%) in RAW264.7 cells compared to the non-treatment group (8.45 ± 1.71%), suggesting the intracellular ROS production in macrophages. Similar to the previous results, ZML treatment significantly reduced the DCF-DA+ area in LPS-induced activated RAW264.7 cells (24.17–7.50%), suggesting that ZML treatment successfully diminished accumulated intracellular ROS, thereby mitigating oxidative stress in macrophages.

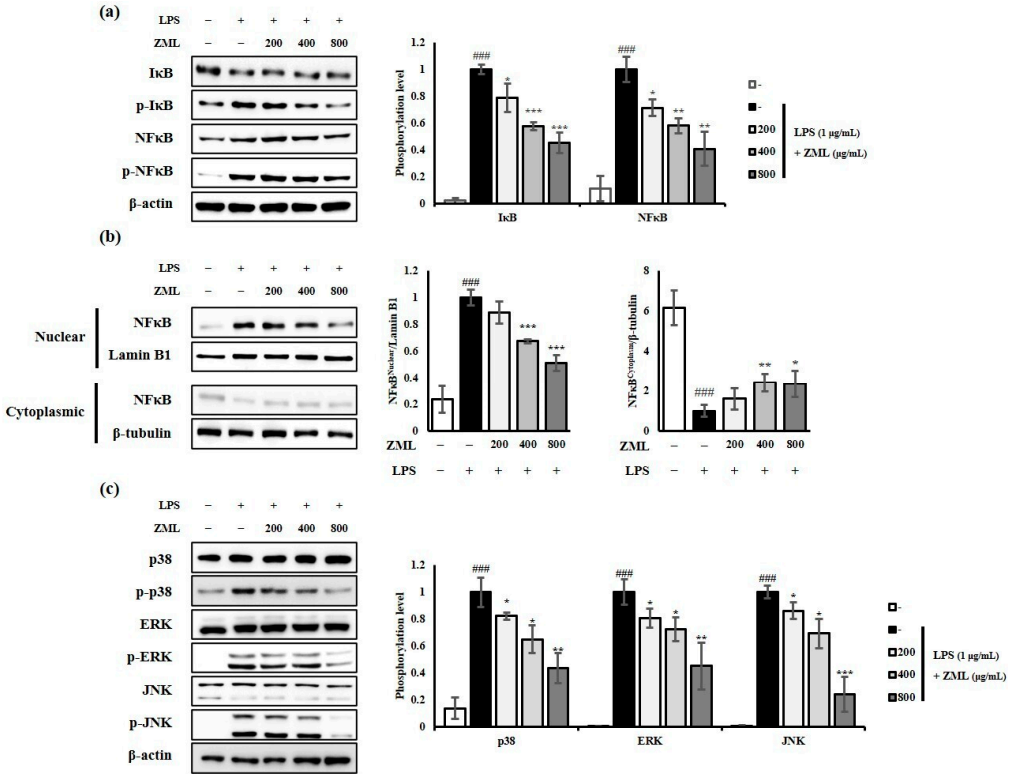


Figure 4. *Zophobas morio* lipid (ZML) alleviated LPS-induced inflammatory responses by downregulating NFκB and MAPK signaling pathways in macrophages. RAW264.7 cells were pretreated with various concentrations of ZML for 1 h, and then co-treated with LPS (1 μg/mL) for 15 min for the NFκB signaling pathway or 30 min for the MAPK signaling pathway. The phosphorylation of IκB and NFκB (**a**), translocation of NFκB (**b**), and MAPK signaling factors (**c**) were analyzed using Western blot analysis. ### $p < 0.001$ compared with the non-treatment group and the LPS-only treatment group. * $p < 0.05$, ** $p < 0.01$, and *** $p < 0.001$ compared with the LPS + ZML co-treatment group and the LPS-only treatment group.

One well-known antioxidant signaling pathway is the nuclear factor E2-related factor 2 (Nrf2) pathway [58]. In the basal state, Nrf2 binds with Kelch-like ECH-associated protein1 (Keap1); however, upon activation, Nrf2 dissociates from Keap1 and translocates into the nucleus [59]. Once in the nucleus, Nrf2 acts as a transcription factor that blocks the transcription of pro-inflammatory cytokines and induces the expression of antioxidant enzymes, such as heme oxygenase-1 (HO-1) [59,60]. Therefore, numerous studies have focused on the Nrf2 signaling pathway to elucidate the antioxidant and anti-inflammatory mechanisms of natural products [14,61,62]. Figures 5b, S4b and S5 refer to the time-dependent activation of the Nrf2 signaling pathway of ZML in macrophages. Notably, overall Nrf2 expression increased continuously over time, suggesting Nrf2 accumulation. Then, the inverse correlation between the decrease in Keap1 expression (peaking at 1 h) and the subsequent increased expression of nuclear Nrf2 (peaking at 2 h) demonstrated Nrf2 nuclear translocation. Consistent with the nuclear translocation of Nrf2, HO-1 expression significantly increased after 2 h and showed a continuous upward trend, confirming the activation of the Nrf2 signaling pathway of ZML in macrophages. These results are consistent with those of the study by Ren et al. [63], which demonstrated that gambogic acid induces HO-1 expression via the Nrf2 signaling pathway, thereby exerting both anti-inflammatory and antioxidant properties.

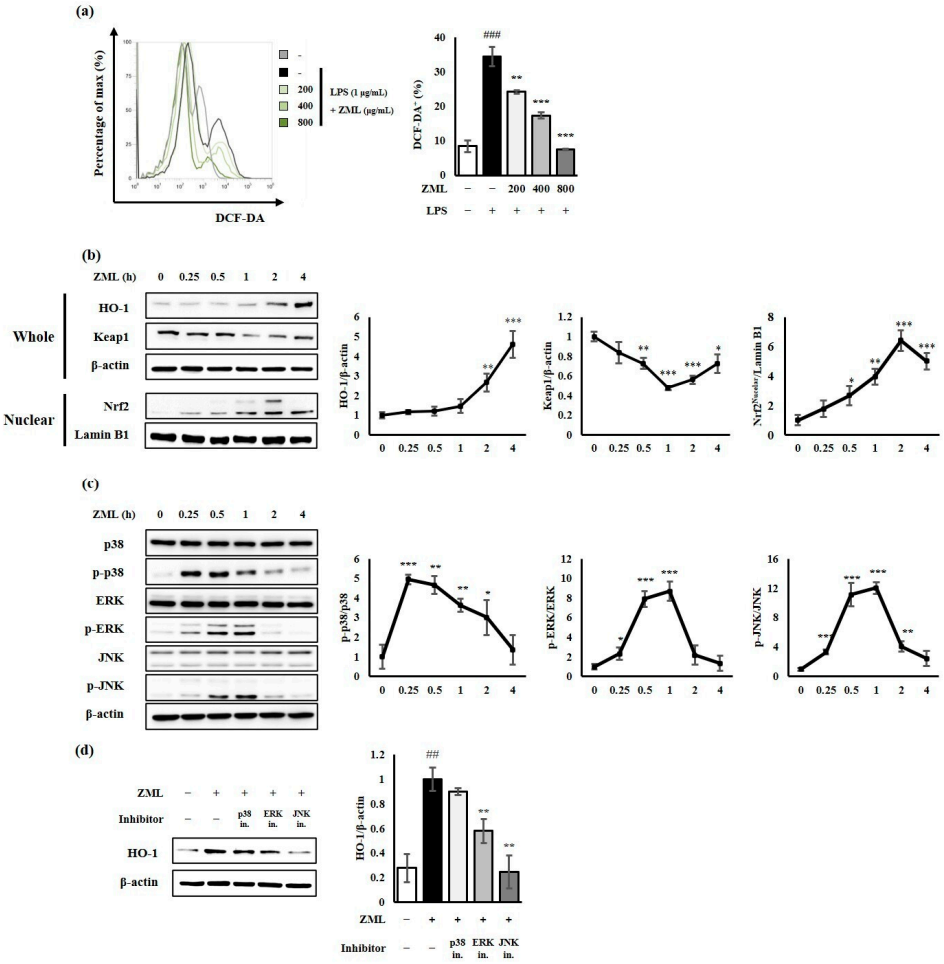


Figure 5. *Zophobas morio* lipid (ZML) ameliorated LPS-induced inflammatory oxidative stress by upregulating MAPK/Nrf2/HO-1 signaling in macrophages. (**a**) RAW 264.7 cells were pretreated with ZML for 1 h, and then co-treated with LPS (1 μg/mL) for 24 h. Intracellular reactive oxygen species production was analyzed using the DCF-DA assay and flow cytometry. (**b**,**c**) RAW264.7 cells were treated with 800 μg/mL of ZML for 0.25–4 h. The expression of MAPK and Nrf2 signaling factors was analyzed by Western blot. (**d**) RAW264.7 cells were pretreated with 20 μM of p38 inhibitor (p38 in; SB203580), ERK inhibitor (ERK in; PD98059), and JNK inhibitor (JNK in; SP600125) for 2 h, and then co-treated with 800 μg/mL of ZML for another 4 h. HO-1 expression was analyzed by Western blot. $^{\#\#}$ $p < 0.01$, $^{\#\#\#}$ $p < 0.001$ compared with the non-treatment group and LPS treatment (**a**) or ZML treatment (**d**) groups. * $p < 0.05$, ** $p < 0.01$, and *** $p < 0.001$ compared with the experimental groups and the respective control groups: LPS-only treatment (**a**), non-treatment (**b**,**c**), or ZML-only treatment group (**d**).

Emerging evidence elucidates that MAPK signaling pathways serve as upstream regulators of Nrf2 activation [64]. Zipper et al. [65] demonstrated that p38 and ERK function as critical upstream regulators of the Nrf2 signaling pathway. In a related study, Xu et al. [66] reported that phosphorylation of ERK and JNK could directly phosphorylate Nrf2, thereby promoting its transcriptional activity. Consequently, numerous studies have focused on targeting the MAPK signaling pathways as a key upstream mechanism to modulate Nrf2-mediated responses [67,68]. Figure 5c,d denote the effects of ZML on the activation of MAPK signaling pathways and their roles in Nrf2-mediated HO-1 expression. As shown in Figure 5c, members of the MAPK signaling pathway were activated at distinct time points. The phosphorylation of p38 reached a peak between 0.25 and 0.5 h, whereas ERK and JNK reached a peak between 0.5 and 1 h. Furthermore, to determine the influence of MAPK signaling on Nrf2-mediated HO-1 expression, pharmacological inhibitors were utilized

(Figure 5d). Compared to the non-inhibited group (1.00 ± 0.10-fold), HO-1 expression was suppressed when MAPK signaling factors were inhibited; notably, this inhibition was significantly more pronounced with ERK and JNK inhibitors (0.58 ± 0.10-fold and 0.25 ± 0.13-fold) than with p38 inhibition (0.90 ± 0.03-fold). These results aligned with the review by Liu et al. [69] who noted that Nrf2 signaling is positively regulated by ERK and JNK rather than p38.

Based on the principle of hormesis, the biphasic modulation of the MAPK signaling by ZML is noteworthy, suggesting a sophisticated protective mechanism in macrophages [70,71]. On the one hand, ZML acts as an anti-inflammatory agent by suppressing excessive LPS-induced MAPK signaling. On the other hand, it functions as a hormetic stressor that triggers the MAPK-mediated Nrf2 signaling pathway. This pre-emptive activation of the Nrf2/HO-1 axis enhances the cellular antioxidant capacity, thereby mitigating inflammation-induced oxidative stress. Importantly, the phosphorylation level of MAPK signaling induced by ZML was significantly lower than that induced by LPS (Figure S6). These findings indicate that ZML acts as a hormetic stimulus, sufficient to trigger the Nrf2-mediated antioxidant defense system without surpassing the threshold required to initiate pathogenic inflammatory responses. Ultimately, these results demonstrate that ZML could protect macrophages from LPS exposure by enhancing acquired resilience.

3.7. ZML Induced M2 Macrophage Polarization in Macrophages

The M1 and M2 paradigms serve as useful ways to categorize the pro- and anti-inflammatory states of macrophages. One major characteristic of macrophages is plasticity, which refers to their remarkable ability to adapt their functional phenotype in response to environmental signals [49]. The M2 macrophage, referred to as an anti-inflammatory phenotypic macrophage, exerts biological activities distinct from those of the M1 macrophage, including tissue homeostasis, anti-inflammatory activities, and angiogenesis [49,72]. Notably, the IL-10 expressed by M2 macrophages plays a pivotal role in anti-inflammatory activities [73]. In addition, arginase-1 (Arg-1) expressed by M2 macrophages metabolizes L-arginine to produce L-ornithine and urea, which play a crucial role in tissue repair [72]. On the surface of these M2 macrophages, CD206, also known as the mannose receptor, is highly expressed and functions in endocytosis and immune homeostasis [74]. In this study, IL-10, Arg-1, and CD206 were utilized as M2 macrophage biomarkers to confirm the effect of ZML on M2 macrophage polarization. Figure 6a,b denote the effect of ZML on M2 macrophage polarization in quiescent macrophages. Notably, ZML treatment significantly increased the expression of CD206, as well as the expression of Arg-1 and IL-10, indicating M2 macrophage polarization.

Given ZML's ability to induce M2 polarization in quiescent macrophages, this study further investigated whether ZML could repolarize pro-inflammatory M1 macrophages toward an anti-inflammatory M2 phenotype. To this end, M1 macrophage polarization was induced by LPS exposure for 24 h following ZML treatment. LPS treatment significantly increased the proportion of M1 macrophages ($CD80^+CD206^-$ cells) (35.39 ± 1.68%) compared to the non-treatment group (7.26 ± 0.78%), indicating successful M1 macrophage polarization. This upregulation was mitigated by ZML treatment (35.17–29.05%), suggesting a reduction in M1-polarized macrophages. It is noteworthy that the proportion of M1/M2 mixed-phenotype macrophages ($CD80^+CD206^+$ cells) was increased by LPS treatment (15.37 ± 0.74%) relative to the non-treatment group (3.23 ± 0.41%), and was further enhanced by ZML treatment (16.78–23.61%) in a dose-dependent manner. These results are presumed to be due to macrophage plasticity. Xue et al. [75] established a spectrum model of macrophage polarization, which transcends the conventional M1/M2 dichotomous polarization model by expanding it into a continuous range of activation states. In addition,

Smith et al. [76] suggested the continuum macrophage polarization model, demonstrating that macrophages exhibit a mixed M1/M2 phenotype morphology during activation rather than adhering to a single, distinct phenotype. Based on this framework and reflecting macrophage plasticity, this mixed phenotype represents a transitional stage during the polarization process. Therefore, it is plausible to interpret the increase in the M1/M2 mixed-phenotype macrophage population following ZML treatment as a phenotypic skewing toward M2. This mechanism is further supported by the result that the proportion of M2 macrophages ($CD80^{-}CD206^{+}$ cells) was higher in the LPS-ZML co-treatment groups (2.68–3.44%) than in the LPS-only group (2.36 ± 0.08%). Given the inherent plasticity of macrophages, the concurrent increase in mixed M1/M2 phenotypic macrophages further suggests a dynamic transition stage during the M2 polarization process induced by ZML. In summary, these findings suggest that ZML not only promotes M2 polarization from a quiescent state but also reprograms M1-polarized macrophages toward an M2 phenotype.

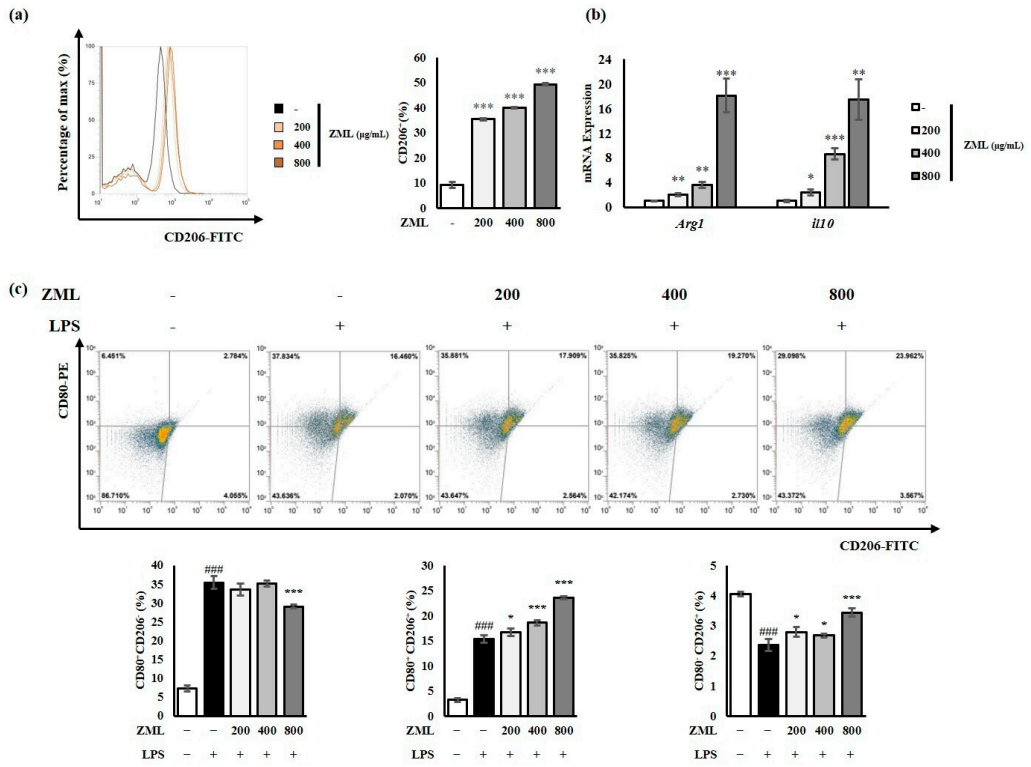


Figure 6. *Zophobas morio* lipid (ZML) induced M2 macrophage polarization in RAW264.7 cells. (**a**,**b**) RAW 264.7 cells were treated with ZML for 24 h; then the expressions of M2 macrophage markers (CD206, Arg1, and IL10) were analyzed using flow cytometry and RT-qPCR. * $p < 0.05$, ** $p < 0.01$, and *** $p < 0.001$ compared with the ZML treatment group and the non-treatment group. (**c**) RAW264.7 cells were treated with LPS (1 μg/mL) for 24 h; subsequently, they were co-treated with ZML for another 24 h. The expression of CD80 and CD206 was analyzed using flow cytometry. ### $p < 0.001$ compared with the non-treatment group and the LPS-only treatment group. * $p < 0.05$ and *** $p < 0.001$ compared with the LPS + ZML co-treatment group and the LPS-only treatment group.

The anti-inflammatory activities of the ZML are attributed to the inhibition of LPS-induced pro-inflammatory M1 macrophage polarization and the promotion of anti-inflammatory M2 macrophage polarization. These results are consistent with previous studies showing that oleic acid, palmitoleic acid, and α-linolenic acid suppress LPS-induced M1 macrophage polarization while promoting M2 macrophage polarization [77–81]. Based on the FA profile of ZML, these specific components are hypothesized to play a significant role in its anti-inflammatory activities (Table 1). In addition to these phenotypic shifts, linoleic acid has been shown to alleviate LPS-induced inflammation by suppressing the

expression of the primary LPS receptor, TLR4, and activating the autophagy pathway [82]. Collectively, these findings suggested that ZML exerts anti-inflammatory activities through a multifaceted regulatory mechanism, in which its diverse constituent fatty acids could act synergistically to elicit a comprehensive biological response ranging from fundamental blockade of inflammatory responses to active orchestration of M1-M2 phenotypic transition. Nevertheless, the specific signaling pathways that drive M2 macrophage polarization, such as the interferon regulatory factors (IRFs) or signaling transducer and activator of transcriptions (STATs) families, remain to be fully elucidated [83,84]. Therefore, further investigations into these key mechanisms are warranted to clarify their roles in the phenotypic transition induced by ZML.

While these specific fatty acids are likely primary contributors, ZML is a complex mixture that also contains other lipid classes, such as phospholipids and sterols. Although not individually identified in this study, these components may collectively contribute to the observed anti-inflammatory activities. Furthermore, as this study was limited to an in vitro model using the specified concentration range, subsequent in vivo studies are necessary to evaluate the systemic efficacy, bioavailability, and safety of ZML. Such investigations will be crucial for determining the effective systemic dosage and bridging the gap between these experimental findings and actual physiological conditions. These findings provide a preliminary basis for further studies using more diverse experimental models to validate the therapeutic potential of ZML.

4. Conclusions

This study characterized the structural and anti-inflammatory properties of ZML. GC-MS, FT-IR, and ^{1}H-NMR analyses revealed a unique structural profile comprising key unsaturated fatty acids (oleic and linoleic acids) and saturated fatty acids (palmitic and stearic acids), providing a molecular basis for its biological activities. TGA and DSC analyses revealed the thermal stability of ZML, further supporting its suitability for various applications. The anti-inflammatory mechanism of ZML involves downregulating NF-κB signaling, upregulating Nrf2/HO-1 signaling, and modulating MAPK signaling pathways. Notably, the observation of MAPK-mediated hormesis provides a more complex understanding of ZML's role in inflammatory conditions. Furthermore, ZML reprograms M1 macrophages to M2 macrophages and induces quiescent macrophages to M2 macrophages, which could promote anti-inflammatory responses and tissue repair. Although this study highlights fatty acid composition and its role in anti-inflammatory properties, further investigation of the potential involvement of other lipid classes, such as complex lipids, sphingolipids, and cholesterol, remains warranted. Consequently, ZML represents a promising bioactive material for anti-inflammatory applications.

Supplementary Materials: The following supporting information can be downloaded at https://www.mdpi.com/article/10.3390/macromol6020021/s1: Figure S1. Standard curve for nitric oxide quantification; Figure S2. Effect of ZML on the cell viability of macrophages; Figure S3. Effect of ZML on the secretion of pro-inflammatory cytokines in LPS-induced activated macrophage; Figure S4. Successful cytosolic/nuclear fractionation performed in the experiment; Figure S5. ZML increased Nrf2 expression in macrophages; Figure S6. Comparison of the effects of ZML and LPS on the phosphorylation levels of MAPK signaling factors; Table S1. Primary antibodies used in Western blot assay; Table S2. Primer sequences used in RT-qPCR analysis; Table S3. FT-IR spectra of ZML; Table S4. ^{1}H-NMR spectra of ZML.

Author Contributions: Conceptualization, J.-H.P., H.-S.C., J.-O.N. and W.-Y.L.; methodology and formal analysis, J.-H.P., H.-S.C., J.-O.N. and W.-Y.L.; investigation, J.-H.P. and H.-S.C.; data curation, J.-H.P. and H.-S.C.; writing—original draft preparation, J.-H.P. and H.-S.C.; writing—review and

editing, J.-O.N. and W.-Y.L.; visualization, J.-H.P. and H.-S.C.; resources and supervision, J.-O.N. and W.-Y.L. All authors have read and agreed to the published version of the manuscript.

Funding: This research received no external funding.

Institutional Review Board Statement: Not applicable.

Data Availability Statement: The original contributions presented in this study are included in the article. Further inquiries can be directed at the corresponding authors.

Conflicts of Interest: The authors declare no conflicts of interest.

Abbreviations

The following abbreviations are used in this manuscript:

ZML	*Zophobas morio* lipids
FA	Fatty acid
FAMEs	Fatty acid methyl esters
FT-IR	Fourier transform infrared spectroscopy
^{1}H-NMR	^{1}Hydrogen-Nuclear magnetic resonance
TGA	Thermogravimetric analysis
DSC	Differential scanning calorimetry
LPS	Lipopolysaccharide
PGE2	Prostaglandin E2
iNOS	Inducible nitric oxide synthase
COX-2	Cyclooxygenase-2
TNF-α	Tumor necrosis factor alpha
IL	Interleukin
CD	Cluster of differentiation
DCF-DA	2′, 7′-dichlorofluorescein diacetate
ROS	Reactive oxygen species
IκB	Inhibitory factor kappa B
NFκB	Nuclear factor kappa B
MAPK	Mitogen-activated protein kinases
HO-1	Hemeoxygenase-1
Keap1	Kelch-like ECH-associated protein 1
Nrf2	Nuclear factor E2-related factor 2
Arg1	Arginase-1

References

1. Fujiwara, N.; Kobayashi, K. Macrophages in inflammation. *Curr. Drug Targets-Inflamm. Allergy* **2005**, *4*, 281–286. [CrossRef]
2. Wynn, T.A.; Chawla, A.; Pollard, J.W. Macrophage biology in development, homeostasis and disease. *Nature* **2013**, *496*, 445–455. [CrossRef]
3. Park, J.H.; Lee, E.; Nam, J.O. Bioconverted extract of Sophorae fructus modulates the innate immune response in RAW264. 7 macrophages and mouse splenocytes. *J. Funct. Foods* **2024**, *116*, 106202. [CrossRef]
4. Park, J.H.; Lee, S.D.; Park, J.J.; Olawuyi, I.F.; Chae, J.; Lee, J.H.; Hwang, J.S.; Lee, W.; Hahn, D.; Nam, J.O. Comparative Analysis of Antioxidant, Macrophage Proliferation, and Nitric Oxide Scavenging Properties of Molecular Weight–Fractionated Polysaccharides Derived From Protaetia brevitarsis seulensis Larvae. *Entomol. Res.* **2025**, *55*, e70063. [CrossRef]
5. Kalinski, P. Regulation of immune responses by prostaglandin E2. *J. Immunol.* **2012**, *188*, 21–28. [CrossRef]
6. Monmai, C.; Kim, J.-S.; Baek, S.-H. Transgenic rice seed extracts exert immunomodulatory effects by modulating immune-related biomarkers in RAW264. 7 macrophage cells. *Nutrients* **2022**, *14*, 4143. [CrossRef]
7. Jeong, H.S.; Bach, T.T.; Paik, J.H.; Jung, S.K. *Cinnamomum longepetiolatum* (Kosterm.) Extract Modulates Inflammatory Responses and Oxidative Stress in Lipopolysaccharide-Stimulated RAW 264.7 Macrophages. *Prev. Nutr. Food Sci.* **2025**, *30*, 459. [CrossRef]
8. Paradkar, P.; Mishra, L.; Joshi, J.; Dandekar, S.; Vaidya, R.; Vaidya, A. In vitro macrophage activation: A technique for screening anti-inflammatory, immunomodulatory and anticancer activity of phytomolecules. *Indian J. Exp. Biol.* **2017**, *55*, 133–141.

9. da Silva Lucas, A.J.; de Oliveira, L.M.; Da Rocha, M.; Prentice, C. Edible insects: An alternative of nutritional, functional and bioactive compounds. *Food Chem.* **2020**, *311*, 126022. [CrossRef]
10. Lumanlan, J.C.; Williams, M.; Jayasena, V. Edible insects: Environmentally friendly sustainable future food source. *Int. J. Food Sci. Technol.* **2022**, *57*, 6317–6325. [CrossRef]
11. Psarianos, M.; Dimopoulos, G.; Ojha, S.; Cavini, A.C.M.; Bußler, S.; Taoukis, P.; Schlüter, O.K. Effect of pulsed electric fields on cricket (*Acheta domesticus*) flour: Extraction yield (protein, fat and chitin) and techno-functional properties. *Innov. Food Sci. Emerg. Technol.* **2022**, *76*, 102908. [CrossRef]
12. Wedamulla, N.E.; Zhang, Q.; Kim, S.-H.; Choi, Y.-J.; Bae, S.M.; Kim, E.-K. Korean edible insects: A promising sustainable resource of proteins and peptides for formulating future functional foods. *Food Suppl. Biomater. Health* **2024**, *4*, e5. [CrossRef]
13. Cho, H.-S.; Park, J.-H.; Olawuyi, I.F.; Nam, J.-O.; Lee, W.-Y. Physicochemical characteristics and anti-inflammatory properties of *Zophobas morio* (super mealworm) protein extracted by different methods. *Food Chem.* **2025**, *468*, 142519. [CrossRef]
14. Cho, H.-S.; Park, J.-H.; Olawuyi, I.F.; Nam, J.-O.; Lee, W.-Y. Optimization of ultrasound-assisted enzymatic hydrolysis *Zophobas morio* protein and its protective effects against H_2O_2-induced oxidative stress in RAW264. 7 cells. *Int. J. Biol. Macromol.* **2025**, *298*, 140111. [CrossRef]
15. Cho, H.-S.; Olawuyi, I.F.; Park, J.-J.; Lee, W.-Y. Quality characteristics of eggless muffins prepared using egg solution alternatives containing super mealworm protein isolate and carrageenan. *Int. J. Food Sci. Technol.* **2023**, *58*, 2942–2948. [CrossRef]
16. Cruz, V.A.; Vicentini-Polette, C.M.; Magalhaes, D.R.; de Oliveira, A.L. Extraction, characterization, and use of edible insect oil—A review. *Food Chem.* **2025**, *463*, 141199. [CrossRef]
17. de la Luz Sánchez-Estrada, M.; Aguirre-Becerra, H.; Feregrino-Pérez, A.A. Bioactive compounds and biological activity in edible insects: A review. *Heliyon* **2024**, *10*, e24045. [CrossRef]
18. dos Santos Aguilar, J.G. An overview of lipids from insects. *Biocatal. Agric. Biotechnol.* **2021**, *33*, 101967. [CrossRef]
19. da Silva, R.M.; Köhler, A.; de Souza Schneider, R.d.C.; de Vargas, D.P.; Köhler, A.L.; e Silva, D.d.C.; Soares, J. Proximate and fatty acid profile analysis of *Tenebrio molitor* and *Zophobas morio* using different killing methods. *Food Chem.* **2024**, *445*, 138719. [CrossRef]
20. Antunes, A.L.M.; Mesquita, B.M.A.d.C.; Fonseca, F.S.A.d.; Carvalho, L.M.d.; Brandi, I.V.; Carvalho, G.G.P.d.; Coimbra, J.S.d.R. Extraction and application of lipids from edible insects. *Crit. Rev. Food Sci. Nutr.* **2025**, *65*, 4651–4659. [CrossRef]
21. Kolobe, S.D.; Manyelo, T.G.; Malematja, E.; Sebola, N.A.; Mabelebele, M. Fats and major fatty acids present in edible insects utilised as food and livestock feed. *Vet. Anim. Sci.* **2023**, *22*, 100312. [CrossRef] [PubMed]
22. Rod-In, W.; Monmai, C.; Lee, S.-M.; Jung, S.-K.; You, S.; Park, W.J. Anti-inflammatory effects of lipids extracted from *Arctoscopus japonicus* eggs on LPS-stimulated RAW264. 7 cells. *Mar. Drugs* **2019**, *17*, 580. [CrossRef] [PubMed]
23. Gwon, Y.G.; Rod-In, W.; Lee, H.J.; Lee, S.-M.; Shin, I.-S.; Park, W.J. Inhibitory effects of *Oncorhynchus mykiss* lipids in LPS-induced RAW264. 7 cells via suppression of NF-κB and MAPK pathways. *Fish Shellfish Immunol.* **2024**, *144*, 109266. [CrossRef] [PubMed]
24. Banskota, A.H.; Stefanova, R.; Sperker, S.; Lall, S.P.; Craigie, J.S.; Hafting, J.T.; Critchley, A.T. Polar lipids from the marine macroalga *Palmaria palmata* inhibit lipopolysaccharide-induced nitric oxide production in RAW264.7 macrophage cells. *Phytochemistry* **2014**, *101*, 101–108. [CrossRef]
25. Wang, L.; Xu, M.L.; Liu, J.; Wang, Y.; Hu, J.H.; Wang, M.-H. Sonchus asper extract inhibits LPS-induced oxidative stress and pro-inflammatory cytokine production in RAW264.7 macrophages. *Nutr. Res. Pract.* **2015**, *9*, 579–585. [CrossRef]
26. Chantakun, K.; Petcharat, T.; Wattanachant, S.; Ab Karim, M.S.B.; Kaewthong, P. Fatty acid profile and thermal behavior of fat-rich edible insect oils compared to commonly consumed animal and plant oils. *Food Sci. Anim. Resour.* **2024**, *44*, 790. [CrossRef]
27. Stark, K.D.; Park, E.J.; Holub, B.J. Fatty acid composition of serum phospholipid of premenopausal women and postmenopausal women receiving and not receiving hormone replacement therapy. *Menopause* **2003**, *10*, 448–455. [CrossRef]
28. Spano, M.; Di Matteo, G.; Fernandez Retamozo, C.A.; Lasalvia, A.; Ruggeri, M.; Sandri, G.; Cordeiro, C.; Sousa Silva, M.; Totaro Fila, C.; Garzoli, S. A multimethodological approach for the chemical characterization of edible insects: The case study of Acheta domesticus. *Foods* **2023**, *12*, 2331. [CrossRef]
29. Cai, S.; Zhang, Y.; Xia, F.; Shen, G.; Feng, J. An expert system based on 1H NMR spectroscopy for quality evaluation and adulteration identification of edible oils. *J. Food Compos. Anal.* **2019**, *84*, 103316. [CrossRef]
30. dos Santos, O.V.; Dias, P.C.S.; Soares, S.D.; da Conceição, L.R.V.; Teixeira-Costa, B.E. Artisanal oil obtained from insects' larvae (*Speciomerus ruficornis*): Fatty acids composition, physicochemical, nutritional and antioxidant properties for application in food. *Eur. Food Res. Technol.* **2021**, *247*, 1803–1813. [CrossRef]
31. Cha, J.Y.; Kim, M.-R.; Kim, Y.-J.; Kim, J.H.; Han, J.; Choi, Y.-S. Influence of the drying method on the physicochemical properties, volatile compounds, and odor characteristics of edible insect oils. *Food Res. Int.* **2025**, *220*, 117088. [CrossRef]
32. Cho, H.-S.; Olawuyi, I.F.; Lee, W.-Y. Comparative extraction and recovery of *Zophobas morio* protein using deep eutectic solvents and conventional alkaline methods: Effects on structure, functionality, and antioxidant properties. *Int. J. Biol. Macromol.* **2025**, *320*, 146107. [CrossRef] [PubMed]

33. Park, J.-H.; Park, J.-J.; Chae, J.; Do Lee, S.; Gwon, S.; Kim, H.; Min, J.H.; Jung, Y.H.; Lee, J.H.; Lee, W. Structural characterization and immune-enhancing properties of an acidic heteroglycan from *Protaetia brevitarsis* seulensis larvae. *Future Foods* **2024**, *10*, 100439. [CrossRef]
34. Perez-Santaescolastica, C.; De Pril, I.; Van de Voorde, I.; Fraeye, I. Fatty acid and amino acid profiles of seven edible insects: Focus on lipid class composition and protein conversion factors. *Foods* **2023**, *12*, 4090. [CrossRef] [PubMed]
35. Mba, A.R.F.; Kansci, G.; Viau, M.; Hafnaoui, N.; Meynier, A.; Demmano, G.; Genot, C. Lipid and amino acid profiles support the potential of Rhynchophorus phoenicis larvae for human nutrition. *J. Food Compos. Anal.* **2017**, *60*, 64–73. [CrossRef]
36. Wang, D.D. Dietary n-6 polyunsaturated fatty acids and cardiovascular disease: Epidemiologic evidence. *Prostaglandins Leukot. Essent. Fat. Acids* **2018**, *135*, 5–9. [CrossRef]
37. Harwood, J.L. Polyunsaturated fatty acids: Conversion to lipid mediators, roles in inflammatory diseases and dietary sources. *Int. J. Mol. Sci.* **2023**, *24*, 8838. [CrossRef]
38. Wu, M.-H.; Wan, L.-Z.; Zhang, Y.-Q. A novel sodium N-fatty acyl amino acid surfactant using silkworm pupae as stock material. *Sci. Rep.* **2014**, *4*, 4428. [CrossRef]
39. Schulz, H.; Baranska, M. Identification and quantification of valuable plant substances by IR and Raman spectroscopy. *Vib. Spectrosc.* **2007**, *43*, 13–25. [CrossRef]
40. Rai, A.; Mohanty, B.; Bhargava, R. Supercritical extraction of sunflower oil: A central composite design for extraction variables. *Food Chem.* **2016**, *192*, 647–659. [CrossRef]
41. Lerma-García, M.J.; Ramis-Ramos, G.; Herrero-Martínez, J.M.; Simó-Alfonso, E.F. Authentication of extra virgin olive oils by Fourier-transform infrared spectroscopy. *Food Chem.* **2010**, *118*, 78–83. [CrossRef]
42. San Martín, E.; Avenoza, A.; Peregrina, J.M.; Busto, J.H. Solvent-based strategy improves the direct determination of key parameters in edible fats and oils by 1H NMR. *J. Sci. Food Agric.* **2020**, *100*, 1726–1734. [CrossRef]
43. Zhang, Y.; Zhao, Y.; Shen, G.; Zhong, S.; Feng, J. NMR spectroscopy in conjugation with multivariate statistical analysis for distinguishing plant origin of edible oils. *J. Food Compos. Anal.* **2018**, *69*, 140–148. [CrossRef]
44. Gomes, A.T.A.; Pereira, R.R.; Duarte Junior, A.P.; da Cruz Rodrigues, A.M.; Remédios, C.M.R.; Brasil, D.d.S.B.; Morais, L.R.B.; Silva-Júnior, J.O.C.; Ribeiro-Costa, R.M. Tucumã (*Astrocaryum vulgare*) fat: An Amazonian material as a pharmaceutical input for lipid nanoparticle production. *J. Therm. Anal. Calorim.* **2022**, *147*, 355–365. [CrossRef]
45. Ribeiro, A.P.B.; Masuchi, M.H.; Miyasaki, E.K.; Domingues, M.A.F.; Stroppa, V.L.Z.; de Oliveira, G.M.; Kieckbusch, T.G. Crystallization modifiers in lipid systems. *J. Food Sci. Technol.* **2015**, *52*, 3925–3946. [CrossRef]
46. Zhou, C.; Gao, J.; Qu, H.; Xu, L.; Zhang, B.; Guo, Q.; Jing, F. Anti-inflammatory mechanism of action of benzoylmesaconine in lipopolysaccharide-stimulated RAW264. 7 cells. *Evid. Based Complement. Altern. Med.* **2022**, *2022*, 7008907.
47. Huang, B.P.; Lin, C.H.; Chen, Y.C.; Kao, S.H. Anti-inflammatory effects of Perilla frutescens leaf extract on lipopolysaccharide-stimulated RAW264. 7 cells. *Mol. Med. Rep.* **2014**, *10*, 1077–1083. [CrossRef]
48. Teng, Y.; Xu, H.; He, X.; Zhuang, Q.; Lu, H.; Xu, R.; Xue, D. LXRα agonist differentially regulates BAFF expression and biological effects in RAW264. 7 cells depending on growth status: LXRα activation and BAFF signaling in RAW264.7 cells. *Biochem. Biophys. Res. Commun.* **2025**, *742*, 151067. [CrossRef]
49. Yan, L.; Wang, J.; Cai, X.; Liou, Y.C.; Shen, H.M.; Hao, J.; Huang, C.; Luo, G.; He, W. Macrophage plasticity: Signaling pathways, tissue repair, and regeneration. *MedComm* **2024**, *5*, e658. [CrossRef]
50. Kim, B.; Lee, J.H.; Seo, M.-J.; Eom, S.H.; Kim, W. Linarin down-regulates phagocytosis, pro-inflammatory cytokine production, and activation marker expression in RAW264.7 macrophages. *Food Sci. Biotechnol.* **2016**, *25*, 1437–1442. [CrossRef]
51. Shiratori, H.; Feinweber, C.; Luckhardt, S.; Wallner, N.; Geisslinger, G.; Weigert, A.; Parnham, M.J. An in vitro test system for compounds that modulate human inflammatory macrophage polarization. *Eur. J. Pharmacol.* **2018**, *833*, 328–338. [CrossRef] [PubMed]
52. Mitchell, S.; Vargas, J.; Hoffmann, A. Signaling via the NFκB system. *Wiley Interdiscip. Rev. Syst. Biol. Med.* **2016**, *8*, 227–241. [CrossRef] [PubMed]
53. Yang, H.; Young, D.W.; Gusovsky, F.; Chow, J.C. Cellular events mediated by lipopolysaccharide-stimulated Toll-like receptor 4: MD-2 is required for activation of mitogen-activated protein kinases and Elk-1. *J. Biol. Chem.* **2000**, *275*, 20861–20866. [CrossRef] [PubMed]
54. Li, X.; Xu, M.; Shen, J.; Li, Y.; Lin, S.; Zhu, M.; Pang, Q.; Tan, X.; Tang, J. Sorafenib inhibits LPS-induced inflammation by regulating Lyn-MAPK-NF-kB/AP-1 pathway and TLR4 expression. *Cell Death Discov.* **2022**, *8*, 281. [CrossRef]
55. Gu, D.H.; Kim, M.J.; Fauziah, A.N.; Jung, S.K. *Craibiodendron stellatum* (Pierre) WW Sm. Extract Suppresses Lipopolysaccharide-Induced Acute Lung Injury by Regulating Macrophage-Mediated Inflammation In Vivo and In Vitro. *J. Med. Food* **2025**, *28*, 934–946. [CrossRef]
56. Kim, S.J.; Kim, S.; Fauziah, A.N.; Park, J.M.; Ryu, J.A.; Yoon, S.R.; Han, C.M.; Jung, S.K. Cirsium setidens Nakai extract and pectolinarin as active compounds promote innate immunity in RAW 264.7 cells and splenocytes. *Appl. Food Res.* **2025**, *5*, 101243. [CrossRef]

57. Han, S.; Gao, H.; Chen, S.; Wang, Q.; Li, X.; Du, L.-J.; Li, J.; Luo, Y.-Y.; Li, J.-X.; Zhao, L.-C. Procyanidin A1 Alleviates Inflammatory Response induced by LPS through NF-κB, MAPK, and Nrf2/HO-1 Pathways in RAW264.7 cells. *Sci. Rep.* **2019**, *9*, 15087. [CrossRef]
58. Liu, M.; Liu, S.; Zhang, Q.; Fang, Y.; Yu, Y.; Zhu, L.; Liu, Y.; Gong, W.; Zhao, L.; Qin, L. Curculigoside attenuates oxidative stress and osteoclastogenesis via modulating Nrf2/NF-κB signaling pathway in RAW264.7 cells. *J. Ethnopharmacol.* **2021**, *275*, 114129. [CrossRef]
59. Ahmed, S.M.U.; Luo, L.; Namani, A.; Wang, X.J.; Tang, X. Nrf2 signaling pathway: Pivotal roles in inflammation. *Biochim. Biophys. Acta (BBA)-Mol. Basis Dis.* **2017**, *1863*, 585–597. [CrossRef]
60. Kobayashi, E.H.; Suzuki, T.; Funayama, R.; Nagashima, T.; Hayashi, M.; Sekine, H.; Tanaka, N.; Moriguchi, T.; Motohashi, H.; Nakayama, K. Nrf2 suppresses macrophage inflammatory response by blocking proinflammatory cytokine transcription. *Nat. Commun.* **2016**, *7*, 11624. [CrossRef]
61. Li, Q.; Qiu, Z.; Wang, Y.; Guo, C.; Cai, X.; Zhang, Y.; Liu, L.; Xue, H.; Tang, J. Tea polyphenols alleviate hydrogen peroxide-induced oxidative stress damage through the Mst/Nrf2 axis and the Keap1/Nrf2/HO-1 pathway in murine RAW264. 7 cells. *Exp. Ther. Med.* **2021**, *22*, 1473. [CrossRef] [PubMed]
62. Qin, T.; Ren, Z.; Liu, X.; Luo, Y.; Long, Y.; Peng, S.; Chen, S.; Zhang, J.; Ma, Y.; Li, J. Study of the selenizing Codonopsis pilosula polysaccharides protects RAW264. 7 cells from hydrogen peroxide-induced injury. *Int. J. Biol. Macromol.* **2019**, *125*, 534–543. [CrossRef]
63. Ren, J.; Li, L.; Wang, Y.; Zhai, J.; Chen, G.; Hu, K. Gambogic acid induces heme oxygenase-1 through Nrf2 signaling pathway and inhibits NF-κB and MAPK activation to reduce inflammation in LPS-activated RAW264. 7 cells. *Biomed. Pharmacother.* **2019**, *109*, 555–562. [CrossRef] [PubMed]
64. Yu, C.; Xu, Y.; Zhao, M.; Song, P.; Yu, J. New insights into mechanism of ellagic acid alleviating arsenic-induced oxidative stress through MAPK/keap1-Nrf2 signaling pathway response, molecular docking and metabolomics analysis in HepG2 cells. *Ecotoxicol. Environ. Saf.* **2024**, *285*, 117029. [CrossRef] [PubMed]
65. Zipper, L.M.; Mulcahy, R.T. Inhibition of ERK and p38 MAP kinases inhibits binding of Nrf2 and induction of GCS genes. *Biochem. Biophys. Res. Commun.* **2000**, *278*, 484–492. [CrossRef]
66. Xu, C.; Yuan, X.; Pan, Z.; Shen, G.; Kim, J.-H.; Yu, S.; Khor, T.O.; Li, W.; Ma, J.; Kong, A.-N.T. Mechanism of action of isothiocyanates: The induction of ARE-regulated genes is associated with activation of ERK and JNK and the phosphorylation and nuclear translocation of Nrf2. *Mol. Cancer Ther.* **2006**, *5*, 1918–1926. [CrossRef]
67. Vrba, J.; Gažák, R.; Kuzma, M.; Papoušková, B.; Vacek, J.; Weiszenstein, M.; Křen, V.; Ulrichová, J. A novel semisynthetic flavonoid 7-O-galloyltaxifolin upregulates heme oxygenase-1 in RAW264. 7 cells via MAPK/Nrf2 pathway. *J. Med. Chem.* **2013**, *56*, 856–866. [CrossRef]
68. Ren, J.; Su, D.; Li, L.; Cai, H.; Zhang, M.; Zhai, J.; Li, M.; Wu, X.; Hu, K. Anti-inflammatory effects of Aureusidin in LPS-stimulated RAW264. 7 macrophages via suppressing NF-κB and activating ROS-and MAPKs-dependent Nrf2/HO-1 signaling pathways. *Toxicol. Appl. Pharmacol.* **2020**, *387*, 114846. [CrossRef]
69. Liu, T.; Lv, Y.-F.; Zhao, J.-L.; You, Q.-D.; Jiang, Z.-Y. Regulation of Nrf2 by phosphorylation: Consequences for biological function and therapeutic implications. *Free Radic. Biol. Med.* **2021**, *168*, 129–141. [CrossRef]
70. Calabrese, E.J.; Kozumbo, W.J. The hormetic dose-response mechanism: Nrf2 activation. *Pharmacol. Res.* **2021**, *167*, 105526. [CrossRef]
71. Lee, J.; Jo, D.-G.; Park, D.; Chung, H.Y.; Mattson, M.P. Adaptive cellular stress pathways as therapeutic targets of dietary phytochemicals: Focus on the nervous system. *Pharmacol. Rev.* **2014**, *66*, 815–868. [CrossRef] [PubMed]
72. Geelhaar-Karsch, A.; Schinnerling, K.; Conrad, K.; Friebel, J.; Allers, K.; Schneider, T.; Moos, V. Evaluation of arginine metabolism for the analysis of M1/M2 macrophage activation in human clinical specimens. *Inflamm. Res.* **2013**, *62*, 865–869. [CrossRef] [PubMed]
73. Wen, Y.; Zhang, S.; Meng, X.; Zhao, C.; Hou, B.; Zhu, X.; Cai, W.; Zhou, Y.; Qiu, L.; Sun, H. Water extracts of Tibetan medicine Wuweiganlu attenuates experimental arthritis via inducing macrophage polarization towards the M2 type. *J. Ethnopharmacol.* **2024**, *318*, 116934. [CrossRef] [PubMed]
74. Jaynes, J.M.; Sable, R.; Ronzetti, M.; Bautista, W.; Knotts, Z.; Abisoye-Ogunniyan, A.; Li, D.; Calvo, R.; Dashnyam, M.; Singh, A. Mannose receptor (CD206) activation in tumor-associated macrophages enhances adaptive and innate antitumor immune responses. *Sci. Transl. Med.* **2020**, *12*, eaax6337. [CrossRef]
75. Xue, J.; Schmidt, S.V.; Sander, J.; Draffehn, A.; Krebs, W.; Quester, I.; De Nardo, D.; Gohel, T.D.; Emde, M.; Schmidleithner, L. Transcriptome-based network analysis reveals a spectrum model of human macrophage activation. *Immunity* **2014**, *40*, 274–288. [CrossRef]
76. Smith, T.D.; Tse, M.J.; Read, E.L.; Liu, W.F. Regulation of macrophage polarization and plasticity by complex activation signals. *Integr. Biol.* **2016**, *8*, 946–955. [CrossRef]

77. Camell, C.; Smith, C.W. Dietary oleic acid increases m2 macrophages in the mesenteric adipose tissue. *PLoS ONE* **2013**, *8*, e75147. [CrossRef]
78. Müller, A.K.; Albrecht, F.; Rohrer, C.; Koeberle, A.; Werz, O.; Schlörmann, W.; Glei, M.; Lorkowski, S.; Wallert, M. Olive oil extracts and oleic acid attenuate the LPS-induced inflammatory response in murine RAW264.7 macrophages but induce the release of prostaglandin E2. *Nutrients* **2021**, *13*, 4437. [CrossRef]
79. Pauls, S.D.; Rodway, L.A.; Winter, T.; Taylor, C.G.; Zahradka, P.; Aukema, H.M. Anti-inflammatory effects of α-linolenic acid in M1-like macrophages are associated with enhanced production of oxylipins from α-linolenic and linoleic acid. *J. Nutr. Biochem.* **2018**, *57*, 121–129. [CrossRef]
80. Pauls, S.D.; Rodway, L.A.; Winter, T.; Taylor, C.G.; Zahradka, P.; Aukema, H.M. Alpha-linolenic acid enhances the phagocytic and secretory functions of alternatively activated macrophages in part via changes to the oxylipin profile. *Int. J. Biochem. Cell Biol.* **2020**, *119*, 105662. [CrossRef]
81. Souza, C.O.; Teixeira, A.A.; Biondo, L.A.; Silveira, L.S.; de Souza Breda, C.N.; Braga, T.T.; Camara, N.O.; Belchior, T.; Festuccia, W.T.; Diniz, T.A. Palmitoleic acid reduces high fat diet-induced liver inflammation by promoting PPAR-γ-independent M2a polarization of myeloid cells. *Biochim. Biophys. Acta (BBA)-Mol. Cell Biol. Lipids* **2020**, *1865*, 158776. [CrossRef]
82. Qin, Y.; Li, K.; Zhang, Q.; Liu, J.; Xie, Y.; Zhang, T.; Wang, X.; Zhang, L.; Jiang, Y.; Liu, G. Linoleic acid inhibits lipopolysaccharide-induced inflammation by promoting TLR4 regulated autophagy in murine RAW264. 7 macrophages. *J. Appl. Biomed.* **2024**, *22*, 185–196. [CrossRef]
83. Chistiakov, D.A.; Myasoedova, V.A.; Revin, V.V.; Orekhov, A.N.; Bobryshev, Y.V. The impact of interferon-regulatory factors to macrophage differentiation and polarization into M1 and M2. *Immunobiology* **2018**, *223*, 101–111. [CrossRef]
84. Chen, S.; Saeed, A.F.; Liu, Q.; Jiang, Q.; Xu, H.; Xiao, G.G.; Rao, L.; Duo, Y. Macrophages in immunoregulation and therapeutics. *Signal Transduct. Target. Ther.* **2023**, *8*, 207. [CrossRef]

Disclaimer/Publisher's Note: The statements, opinions and data contained in all publications are solely those of the individual author(s) and contributor(s) and not of MDPI and/or the editor(s). MDPI and/or the editor(s) disclaim responsibility for any injury to people or property resulting from any ideas, methods, instructions or products referred to in the content.